

Adaptive Control of Solid State Transformer Using Type-2 Fuzzy Neural System

Hakan ACIKGOZ¹, O. Fatih KECECIOGLU², Israfil KARADOL¹, Ahmet GANI², Mustafa SEKKELI²

¹Kilis Aralik University,

Department of Electrical Science, Kilis, 79000, Turkey

hakanacikgoz@kilis.edu.tr (*Corresponding author), israfilkaradol@kilis.edu.tr

²K.Maras Sutcu Imam University,

Department of Electrical and Electronics Engineering, K.Maras, 46100, Turkey

fkececioglu@ksu.edu.tr, agani@ksu.edu.tr, msekkeli@ksu.edu.tr

Abstract: Solid State Transformer (SST), considered as one of the emerging technologies, has a very important place in future electrical energy systems since it has many excellent features such as low volume/weight, controllability, active and reactive power control, voltage regulation, harmonic filtering, reactive power compensation. Considering all these superior features, it is inevitable that there are many designs and control strategies for SSTs. In recent years, many studies have been carried out for SSTs. These studies are generally based on control strategies and schemes. In this study, type-2 fuzzy neural system (T2FNS) which has nonlinear and robust structure has been proposed and investigated for SST. The mathematical models and control schemes of SST including input, isolation and output stages are explained in detail. Then, PI controller, type-1 fuzzy neural system (T1FNS) and T2FNS are designed to control three stages of SST. In order to investigate the dynamic performance of SST based on T2FNS, simulation studies have been realized under input voltage harmonics, unbalanced input voltages and voltage sag/swell conditions in MATLAB/Simulink environment.

Keywords: Solid state transformers, Transformers, Type-1 fuzzy neural system, Type-2 fuzzy neural system

1. Introduction

Electricity generation, as one of the main types of energy, faces a challenge since fossil fuels, which are the main sources of electricity generation are more and more decreasing at the present time.

Moreover, the rapid reduction of fossil fuel resources requires the search for alternative sources of energy to find a solution for future energy production. With the developing technology, the rising living standards and the increasing population, the requirement of electric energy is increasing day by day [1,3]. It is well-known that electricity is provided to consumers by passive transformers, transmission lines, and substations. Classic transformers are one of the most indispensable devices in modern electrical distribution systems. These transformers possess various superior features such as low cost, simple construction, high reliability and efficiency. But these transformers have many disadvantages such as large size and weight, power quality problems, sensitivity to harmonics, lack of self-protection, environmental problems related to oil leaks, and voltage and current uncontrollability.

New technological solutions are required to eliminate these problems. In addition, efforts to develop transformers with technological advances have been increasing rapidly in recent years [1, 4, 6, 10]. New type transformers, which are considered as one of these technological developments, are called as solid state transformer (SST), intelligent universal transformer (IUT) or electronic power transformer (EPT) [11]. When compared to conventional transformers, SSTs possess many important characteristic features such as reduced size and weight, instantaneous voltage regulation, voltage sag and swell compensation, power factor correction, fault isolation, harmonic isolation and environmental benefit [9, 10].

Although SSTs were first proposed by Mc Murray in 1970, the studies on these transformers has shown intense interest during the last 20 years [11]. The aim of all studies is to design a transformer which can carry out all the properties of classical transformers in a single circuit and consisting of completely semiconductor elements [1, 5]. Moreover,

the most important purposes of these studies are to obtain the following characteristics from the transformer structure: power factor correction, voltage sag/swell compensation, fault isolation, fixed output voltage. In order to achieve these purposes, scientists and academics have made many studies and published articles on the design and control of SSTs [1, 4, 5]. The selection of the appropriate topology is an important issue for SST implementation. In Ref. [4], four SST configurations are discussed and compared with each other. In addition, the advantages and disadvantages of these structures have been emphasized and evaluated. Many adaptive controllers are proposed for the control of SST structures. In Ref. [10], linear-quadratic regulator (LQR) based electronic power transformer structure was discussed and simulation study was performed to test the performance of the proposed controller against disturbances. In Ref. [5], SST structures with PI controller, LQR and sliding mode controller are compared in many conditions such as unbalanced input voltage, voltage flicker, voltage sags/swells and voltage harmonics. SST structure with neuro-fuzzy controller was discussed and evaluated. A detailed small signal analysis of the SST structure was performed in Ref. [1]. Ref. [9] suggested the model predictive current controller in order to control the output stage of SST. In Ref. [6], conventional transformers and SSTs are compared in terms of efficiency, weight, volume. The performance characteristics of SST are presented in detail.

Conventional control methods have used in numerous applications in order to control dynamic systems. These conventional methods provide various ways to design a controller based on the mathematical model of system. However, if the model of the system has highly nonlinear structure, the performance of conventional control methods may decrease [1].

The fuzzy logic concept was firstly proposed by Zadeh in 1965 [15]. Nowadays, Fuzzy Logic Systems (FLSs) have been successfully performed in various engineering applications including control, robotics, signal processing, pattern recognition, estimation and modelling. Type-1 fuzzy logic systems (T1FLSs) have limitations in the ability of expressing the uncertainties and nonlinearities.

These limitations are relatively occurred because the membership grade for each input value has a crisp value [2, 7, 8, 12-14]. The Type-2 Fuzzy Logic Systems (T2FLSs) which is an extended form of T1FLSs, are used in many studies for controller design. Recently, many studies have been implemented for investigate the internal structure and stability analysis of the T2FLSs. Fuzzy logic systems are usually combined with artificial neural systems (ANNs) and these systems are called as fuzzy neural systems (FNSs) [12-14]. These systems have all the features of both techniques. In this study, Type-2 Fuzzy Neural System (T2FNS) which has the advantages of T2FLS and ANN is proposed for SST.

This article presents the mathematical modelling and robust controller design for SST structure. The mathematical model and operation principles of SST, including input, isolation and output stages are comprehensively described in section 2. T2FNS is proposed to control the input, isolation and output stages of SST in section 3. In section 4, the simulation studies have been realized to verify the dynamic performance of the SST structure with T2FNS in MATLAB/Simulink environment. Then, input voltage harmonics, unbalanced input voltages and voltage sag/swell conditions have been applied to SST structure.

2. Mathematical Model of SST

The voltage equations of input, isolation and output stages of SST structure are given as follows [1, 5]:

$$\begin{bmatrix} u_a(t) \\ u_b(t) \\ u_c(t) \end{bmatrix} = \sqrt{2}U_s \begin{bmatrix} \sin \omega t \\ \sin(\omega t - 120) \\ \sin(\omega t + 120) \end{bmatrix} \quad (1)$$

$$\begin{bmatrix} u_{ia}(t) \\ u_{ib}(t) \\ u_{ic}(t) \end{bmatrix} = m_1 U_{dc} \begin{bmatrix} \sin(\omega t - \theta_1) \\ \sin(\omega t - 120 - \theta_1) \\ \sin(\omega t + 120 - \theta_1) \end{bmatrix} \quad (2)$$

$$\begin{bmatrix} u_{oa}(t) \\ u_{ob}(t) \\ u_{oc}(t) \end{bmatrix} = m_2 U_{dc} \begin{bmatrix} \sin(\omega t - \theta_2) \\ \sin(\omega t - 120 - \theta_2) \\ \sin(\omega t + 120 - \theta_2) \end{bmatrix} \quad (3)$$

The differential equations of SST structure can be written in matrix forms as:

$$L \frac{d}{dt} \begin{bmatrix} i_{ia}(t) \\ i_{ib}(t) \\ i_{ic}(t) \end{bmatrix} = \begin{bmatrix} u_{sa}(t) \\ u_{sb}(t) \\ u_{sc}(t) \end{bmatrix} - \begin{bmatrix} u_{ia}(t) \\ u_{ib}(t) \\ u_{ic}(t) \end{bmatrix} - R \begin{bmatrix} i_{ia}(t) \\ i_{ib}(t) \\ i_{ic}(t) \end{bmatrix} \quad (4)$$

$$C_f \frac{d}{dt} \begin{bmatrix} u_{La}(t) \\ u_{Lb}(t) \\ u_{Lc}(t) \end{bmatrix} = \begin{bmatrix} i_{fa}(t) \\ i_{fb}(t) \\ i_{fc}(t) \end{bmatrix} - \begin{bmatrix} i_{La}(t) \\ i_{Lb}(t) \\ i_{Lc}(t) \end{bmatrix} \quad (6)$$

$$L_f \frac{d}{dt} \begin{bmatrix} i_{fa}(t) \\ i_{fb}(t) \\ i_{fc}(t) \end{bmatrix} = \frac{1}{k} \begin{bmatrix} u_{oa}(t) \\ u_{ob}(t) \\ u_{oc}(t) \end{bmatrix} - \begin{bmatrix} u_{La}(t) \\ u_{Lb}(t) \\ u_{Lc}(t) \end{bmatrix} \quad (5)$$

$$\frac{d}{dt} \left(\frac{1}{2} C_{dc}^2(t) \right) = \begin{bmatrix} u_{ia}(t) & u_{ib}(t) & u_{ic}(t) \end{bmatrix} \begin{bmatrix} i_{ia}(t) \\ i_{ib}(t) \\ i_{ic}(t) \end{bmatrix} - \frac{1}{k} \begin{bmatrix} u_{oa}(t) & u_{ob}(t) & u_{oc}(t) \end{bmatrix} \begin{bmatrix} i_{fa}(t) \\ i_{fb}(t) \\ i_{fc}(t) \end{bmatrix} \quad (7)$$

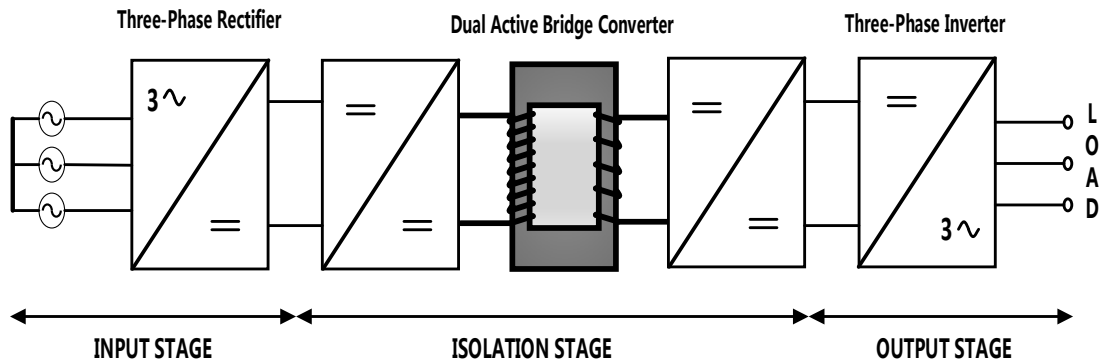


Figure 1. Configuration of SST

where, m_1 and m_2 are amplitude modulation indexes of PWM rectifier and three-phase inverter, respectively. Θ_1 and Θ_2 are modulation angles of PWM rectifier and inverter, respectively. The grid voltages are shown as u_a , u_b and u_c . Output voltages are given as u_{La} , u_{Lb} and u_{Lc} . The input stage DC voltage is symbolized as U_{DC} . u_{oa} , u_{ob} and u_{oc} are the output stage voltages. u_{ia} , u_{ib} and u_{ic} are the input stage voltages. In three-phase stationary reference frame, dynamic model of SST structure can be written by equations (1) to (7). However, the parameters of the dynamic differential equations must be transformed into synchronized rotating reference frame using the Park transformer to obtain time-varying and time invariant equations. Therefore, the equations in d-q rotating reference frame can be shown as follows [1, 5]:

$$\frac{d}{dt} \begin{bmatrix} i_{ld}(t) \\ i_{lq}(t) \end{bmatrix} = -\frac{R}{L} \begin{bmatrix} i_{ld} \\ i_{lq} \end{bmatrix} - \omega \begin{bmatrix} i_{lq} \\ -i_{ld} \end{bmatrix} + \frac{m_1}{L} u_{dc} \begin{bmatrix} \sin \theta_1 \\ \cos \theta_1 \end{bmatrix} + \frac{\sqrt{2}}{L} \begin{bmatrix} 0 \\ u_s \end{bmatrix} \quad (8)$$

$$\frac{d}{dt} [u_{dc}] = -\frac{3m_1}{2C} \begin{bmatrix} i_{ld} \sin \theta_1 \\ -i_{lq} \cos \theta_1 \end{bmatrix} + \frac{3m_2}{2kC} \begin{bmatrix} i_{fd} \sin \theta_2 \\ -i_{fq} \cos \theta_2 \end{bmatrix} \quad (9)$$

$$\frac{d}{dt} \begin{bmatrix} u_{Ld} \\ u_{Lq} \end{bmatrix} = \frac{1}{C_f} \begin{bmatrix} i_{fd} \\ i_{fq} \end{bmatrix} - \frac{1}{C_f} \begin{bmatrix} i_{Ld} \\ i_{Lq} \end{bmatrix} - \omega \begin{bmatrix} u_{Lq} \\ -u_{Ld} \end{bmatrix} \quad (10)$$

$$\frac{d}{dt} \begin{bmatrix} i_{fd} \\ i_{fq} \end{bmatrix} = \omega \begin{bmatrix} -i_{fq} \\ i_{fd} \end{bmatrix} + \frac{m_2 \sin \theta_2}{kL_f} \begin{bmatrix} -u_{dc} \\ u_{dc} \end{bmatrix} - \frac{1}{L_f} \begin{bmatrix} u_{Ld} \\ u_{Lq} \end{bmatrix} \quad (11)$$

functions of rule j for input i and described as Gaussian membership function b_j and w_{ij} are the parameters of network for T1FLS. The membership function of each member of primary parts is represented by upper and lower membership functions. The following equation can be written for these membership functions.

$$\mu_{\tilde{A}_k} (x_k) = [\underline{\mu}_{\tilde{A}_k} (x_k), \bar{\mu}_{\tilde{A}_k} (x_k)] = [\underline{\mu}^i, \bar{\mu}^i] \quad (15)$$

In general, the implied operator in the inference engine is selected as "min" or "prod" t-norms. As seen from the following equation, the latter is selected to obtain the firing strengths.

$$\begin{aligned} \underline{f} &= \underline{\mu}_{\tilde{A}_1} (x_1) * \underline{\mu}_{\tilde{A}_2} (x_2) * \dots * \underline{\mu}_{\tilde{A}_n} (x_n) \\ \bar{f} &= \bar{\mu}_{\tilde{A}_1} (x_1) * \bar{\mu}_{\tilde{A}_2} (x_2) * \dots * \bar{\mu}_{\tilde{A}_n} (x_n) \end{aligned} \quad (16)$$

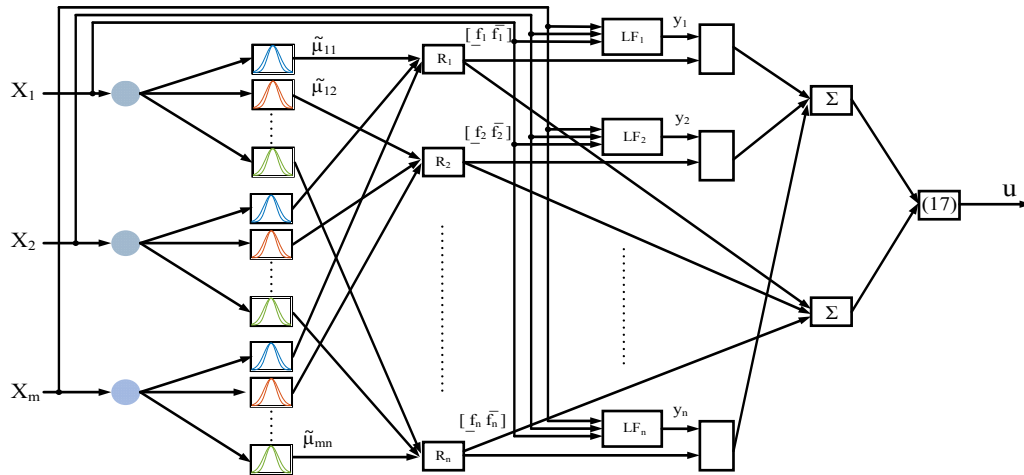


Figure 3. The architecture of type-2 FNS

The next step is type reduction and defuzzification operations. Equation (16) is used for identification of the firing strengths of rules. In order to define the output of type-2 TSK FNS, the inference engine proposed in [2, 8] is employed.

$$u = \frac{q \sum_{j=1}^N \underline{f}_j y_j + (1-q) \sum_{j=1}^N \bar{f}_j y_j}{\sum_{j=1}^N \underline{f}_j + \sum_{j=1}^N \bar{f}_j} \quad (17)$$

$$y_j = \sum_{i=1}^m x_j \omega_{ij} + b_i \quad (i=1 \text{ to } n; j=1 \text{ to } m) \quad (18)$$

where, N describes the number of active rules, and are obtained from equation (14), determination of is held by equation (16) and q is a specified factor in design states the contributions of lower and upper values.

Architecture of T2FNS using Gaussian membership functions as:

$$\mu(x) = \exp\left(-\frac{1}{2} \frac{(x-c)^2}{\sigma^2}\right) \quad (19)$$

where, c and σ exhibit the center and the widths of membership functions for input

vector x . c and σ parameters are found at certain intervals. Input signals are given in Layer 1 of Figure 3. Layer 2 contains linguistic terms for each of nodes. In layer 2, determination of membership degrees $\bar{\mu}(x)$ and $\underline{\mu}(x)$ are obtained from equation (19) for each input signal. Layer 3 employs the product progress determined in equation (16). Layer 4 demonstrates the determination of linear functions outputs given in equation (18) for consequent parts. The layer 5 calculates the multiplication of membership degrees $\bar{f}_j, \underline{f}_j$ and linear y_i functions [7, 12]. Layer 6 consists of pairs of total blocks which perform the calculation sum of the outputs of layer 5 as the numerators of equation (17) sum of the Layer 4 outputs the denominator of equation (17).

Lastly, layer 7 calculates the output of the whole system via equation (17) [13]. In this paper, architecture of T2FNS is chosen using clustering method [7]. The membership and cluster centers can be obtained as follows [13]:

$$u_j(x_i) = \left[\sum_{k=1}^c \left(\frac{d_{ji}}{d_{ki}} \right)^{2/(m-1)} \right]^{-1} \tag{20}$$

$$c_j = \frac{\sum_{i=1}^I x_i (u_j(x_i))^m}{\sum_{i=1}^I (u_j(x_i))^m}$$

where, i is the number of input samples, $u_j(x_i)$ is value of the membership function belongs to x_i pattern in cluster j , $d_{ji}(d_{ki})$ states the distances among clusters, x_i and $c_j(c_k)$ point. Lastly, m controls the fuzziness in fuzzy classification as a fuzzifier. Primary memberships of interval type-2 fuzzy sets for x_i data point are given as [13]:

$$\bar{u}_j(x_i) = \begin{cases} \frac{1}{\sum_{k=1}^c \left(\frac{d_{ji}}{d_{ki}} \right)^{\frac{2}{m_1}}}; & \text{If } \frac{1}{\sum_{k=1}^c \left(\frac{d_{ji}}{d_{ki}} \right)^{\frac{2}{m_1}}} > \frac{1}{\sum_{k=1}^c \left(\frac{d_{ji}}{d_{ki}} \right)^{\frac{2}{m_2}}} \\ \frac{1}{\sum_{k=1}^c \left(\frac{d_{ji}}{d_{ki}} \right)^{\frac{2}{m_2}}}; & \text{Otherwise} \end{cases} \tag{21}$$

$$\underline{u}_j(x_i) = \begin{cases} \frac{1}{\sum_{k=1}^c \left(\frac{d_{ji}}{d_{ki}} \right)^{\frac{2}{m_1}}}; & \text{If } \frac{1}{\sum_{k=1}^c \left(\frac{d_{ji}}{d_{ki}} \right)^{\frac{2}{m_1}}} \leq \frac{1}{\sum_{k=1}^c \left(\frac{d_{ji}}{d_{ki}} \right)^{\frac{2}{m_2}}} \\ \frac{1}{\sum_{k=1}^c \left(\frac{d_{ji}}{d_{ki}} \right)^{\frac{2}{m_2}}}; & \text{Otherwise} \end{cases} \tag{22}$$

where, $d_{ji}(d_{ki})$ states the distances among clusters, x_i and $c_j(c_k)$ point, C is number of clusters, $\underline{u}_j(x_i)$ and $\bar{u}_j(x_i)$ are the lower and upper memberships. Using two different fuzzifiers m_1 and m_2 come with following functions to be minimized:

$$J_{m_1} = \sum_{i=1}^N \sum_{j=1}^C u_{ij}^{m_1} d_{ji}^2 \tag{23}$$

$$J_{m_2} = \sum_{i=1}^N \sum_{j=1}^C u_{ij}^{m_2} d_{ji}^2$$

Here, $1 \leq m_1 \leq m_2 \leq \infty$. It can be used employing m in equation (24) while secondary membership function is equal to one, following equation can be given as [13]:

$$c_x = [c_L \ c_R] = \frac{\sum_{u(x_i) \in x_L} \dots \sum_{u(x_i) \in x_R} \frac{1}{\sum_{i=1}^I x_i u(x_i)^m}}{\sum_{i=1}^I u(x_i)^m} \tag{24}$$

where, $c_L \leq \forall c_j \leq c_R$.

Defuzzification determines the crisp center as [13]:

$$c_j = (c_L + c_R) / 2 \tag{25}$$

Primarily, output error is achieved in equation (26):

$$E = \frac{1}{2} \sum_{i=1}^O (u_i^d - u_i)^2 \tag{26}$$

Here, O is output number of network and in our system $O=I$. u_i^d and u_i present the desired and actual outputs of network. Other parameters b_j , w_{ij} , $c1_{ij}$, $c2_{ij}$ and σ_{ij} are set using followings:

$$\omega_{ij}(t+1) = \omega_{ij}(t) - \gamma \frac{\partial E}{\partial \omega_{ij}} \tag{27}$$

$$b_j(t+1) = b_j(t) - \gamma \frac{\partial E}{\partial b_j}$$

Here, γ is learning rate, m is input neurons of network and n is number of hidden neurons. Included derivatives in equation (27) can be calculated using following [13]:

$$\frac{\partial E}{\partial b_j} = \frac{\partial E}{\partial u} \frac{\partial u}{\partial y_j} \frac{\partial y_j}{\partial b_j} \tag{28}$$

$$\frac{\partial E}{\partial b_j} = (u(t) - u^d(t)) \left(\frac{q \cdot f_{-j}}{\sum_{j=1}^n f_{-j}} + \frac{(1-q) \cdot \bar{f}_j}{\sum_{j=1}^n \bar{f}_j} \right) \tag{29}$$

The expression belongs to t-norm prod operator is given as [13]:

$$\frac{\partial f_j}{\partial \underline{\mu}_{ij}} = \prod_{k=1}^{N1} \mu_{kj} ; \frac{\partial \bar{f}_j}{\partial \bar{\mu}_{ij}} = \prod_{k=1}^{N1} \bar{\mu}_{kj} \tag{30}$$

$$\underline{\mu}_{ij}(x) = \begin{cases} G(c2_{ij}, \sigma_{ij}, x_i); & x_i \leq \frac{c1_{ij} + c2_{ij}}{2} \\ G(c1_{ij}, \sigma_{ij}, x_i); & x_i > \frac{c1_{ij} + c2_{ij}}{2} \end{cases} \tag{31}$$

Where, $i=1, \dots, N1$, $k=1, \dots, N1$, $j=1, \dots, N2$. Upper and lower membership functions in layer 3 coupling input i and output j are given as [9]:

$$\bar{\mu}_{ij}(x) = \begin{cases} G(c1_{ij}, \sigma_{ij}, x_i); & x_i < c1_{ij} \\ 1; & c1_{ij} \leq x_i \leq c2_{ij} \\ G(c2_{ij}, \sigma_{ij}, x_i); & x_i > c2_{ij} \end{cases} \quad (32)$$

Here, $G(c_{ij}, \sigma_{ij}, x_i)$ can be stated as

$$G(c_{ij}, \sigma_{ij}, x_i) = \exp\left(-\frac{1}{2} \frac{(x_i - c_{ij})^2}{\sigma_{ij}^2}\right) \quad (33)$$

Using equation (27) coupled with equations (28)-(33), T2FNS parameters are updated [13].

4. Simulation Studies

In order to verify the performance of SST structure, simulations studies have been performed under conditions of voltage harmonics, voltage flicker, unbalanced input voltages, voltage sag and swell in condition Matlab/Simulink environment. The T2FNS with the proposed structure is implemented on the input, isolation and output stages of SST.

Also, PI controller and T1FNS are designed to better demonstrate the performance of SST based on proposed controller. The SST structure is designed as 4 kV three-phase input voltage and 400 V DC output. The proposed SST structure consists of an three-phase rectifier that converts 4 kV AC to 10 kV DC bus voltage, a dual active bridge converter that convert 10 kV to 400V DC voltage and

three-phase inverter that converts 400V DC to 220V AC. The SST parameters used in this study are detailed in Table 1. Also, the simulation model of SST is given Figure 4.

The first performance test is realized in order to demonstrate impact of three controllers for voltage harmonics of the 5th and 7th orders with amplitudes of 15% and 20%. The waveforms obtained from this test are given Figure 5.

The DC bus voltage responses of input stage for three controller structures are regulated to the reference 10 kV. As can be seen in Figure 5b, harmonics condition happens between t=0.3 and t=0.4 s, DC bus voltage responses of PI controller, T1FNS and T2FNS increase to 10.06 kV, 10.02 kV and 10.015 kV, respectively. Despite this condition, the effect of voltage harmonics has been removed in the SST structure.

Table 1. SST Simulation Parameters

Description	Value
Grid AC Voltage	4 kV
Line inductance (L)	100 mH
DC capacitor of Input Stage	30 μ F
High voltage DC Voltage	10 kV
DC capacitor of Output Stage	2 mF
Low voltage DC Voltage	400 V
Sampling time	50 μ s

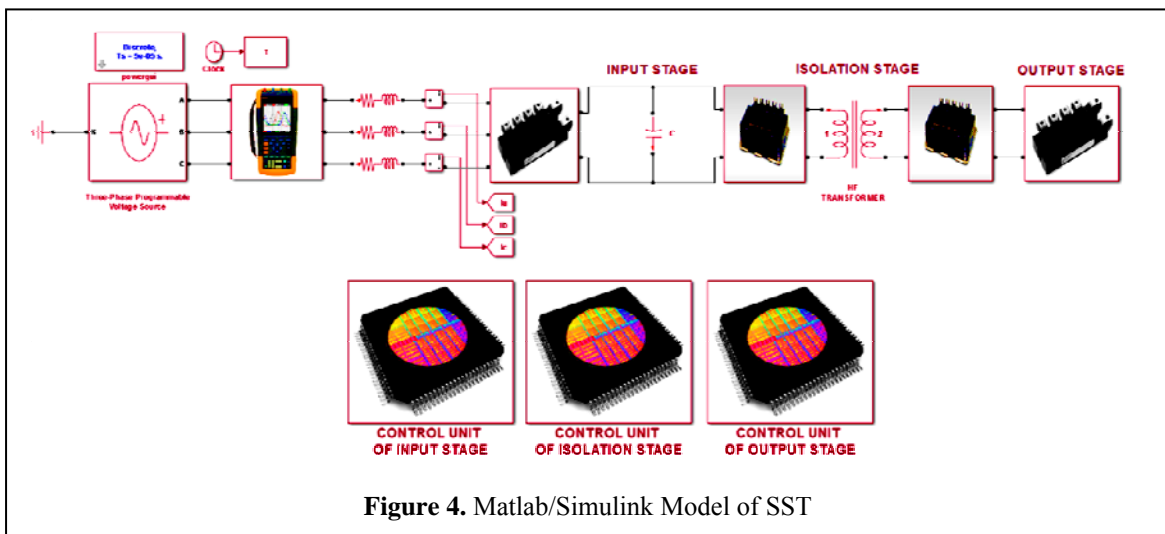


Figure 4. Matlab/Simulink Model of SST

Additionally, Figure 5c shows that the output voltage is still sinusoidal despite voltage harmonics. Consequently, SST structure with T2FNS improves the overall performances when compared to PI controller and T1FNS. The second performance test is carried out to indicate response of SST structure for voltage sag condition. One of the most important features of the SST structure is the voltage sag and swell compensation ability. As can be seen in Figure 6, the magnitude of grid voltage decreases from 100% to 65% at 0.3s, and then increases from 65% to 100% at 0.4s. During this condition, DC bus voltages of input stage obtained from PI controller and T1FNS are 9.92 kV and 9.98 kV while DC bus voltage with proposed controller is 9.99 kV. Figure 6c demonstrates the output voltage response of SST structure under voltage sag. As shown in the Figure 6c, the output voltage is not affected by voltage sag condition. The voltage sag can be compensated by the SST structure. As a result of this performance test, SST structure with T2FNS is more stable than PI controller and T1FNS because of its robust structure against disturbances and uncertainties. The third performance test is performed to show response of SST structure for voltage swell condition. As shown in Figure 7a, the magnitude of grid voltage increases from 100% to 125% at 0.3s, and then decreases from 125% to 100% at 0.4s. As shown in Figure 7b, DC bus voltage responses of input stage obtained from PI controller and T1FNS increase from 10 kV to 10.09 kV and from 10 kV to 10.02 kV, respectively while DC bus voltage with T2FNS increases from 10 kV to 10.015 kV. The SST with T2FNS has less overshoot/undershoot and follows the reference voltage faster than PI controller and T1FNS. As shown in the Figure 7c, the output voltage is not influenced by voltage swell and the voltage swell condition can be compensated by the SST structure. Consequently, it can be concluded that the proposed controller improves the overall performances in general comparing to PI controller and and T1FNS. The last performance test is carried out to demonstrate response of SST structure for unbalanced input voltage condition. As can be seen from Figure 8a, the voltage amplitude of phase A has 40% voltage sag, the frequency of phase-B is adjusted to 48 Hz, the angle of phase C is 85°.

The DC bus voltage responses of input stage can be seen in Figure 8b when for unbalanced input voltage condition is applied. As can be seen, DC bus undershoot voltages of PI controller and T1FNS are almost 75 V and 25 V, respectively. PI controller and T1FNS follow the reference DC bus voltage after 0.2 and 0.145 s, respectively. DC bus undershoot voltage of T2FNS is nearly 23 V and follows the reference DC bus voltage after 0.14 s. As seen, oscillations on the DC bus voltage response obtained from T2FNS are nearly vanished more quickly compared to the PI controller and T1FNS. As expected from SST structure, the output voltages are still sinusoidal. The obtained results are clearly demonstrated that SST structure with performance of whole power system. T2FNS are nearly vanished more quickly compared to the PI controller and T1FNS. As expected from SST structure, the output voltages are still sinusoidal. The obtained results are clearly demonstrated that SST structure with T2FNS is improved significantly the performance of whole power system.

5. Conclusion

With technological developments, many control algorithms are carried out on SST structures because of their additional features such as high power factor, low harmonic distortion, constant output voltage and reactive power compensation. In this work, SST structure consisting of three stages is designed in the Matlab/Simulink environment. A T2FNS has been proposed to control the sections of this SST structure because of its superior performance against disturbances and uncertainties. Then, the designed T2FNS was applied to the SST structure. Many simulation studies have been realized in order to confirm the performance of SST structure based on T2FNS. All performance test results show that T2FNS has improved the performance and stability of the SST structure.

Acknowledgements

This work was financially supported by the Kahramanmaraş Sutcu Imam University, Scientific Research Projects Unit under Project No: 2016/3-52D and 2017/1-81M.

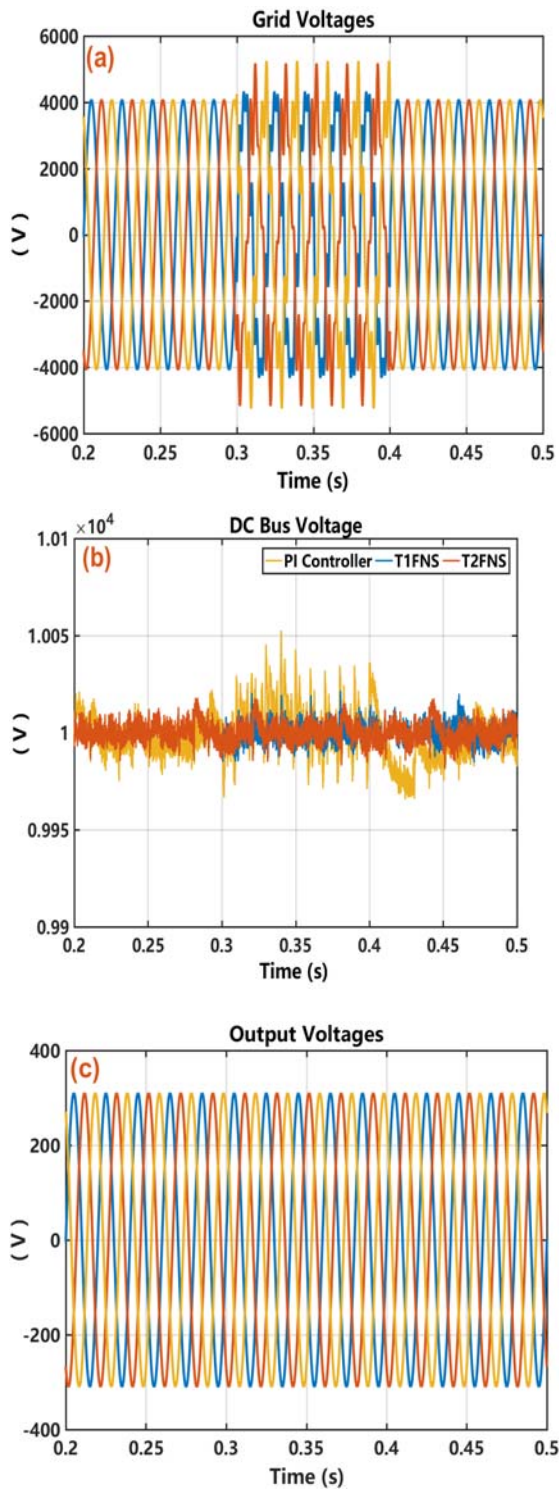


Figure 5. Waveforms obtained from the first performance test a) Grid voltages b) DC-bus voltages of input stage c) Output voltages

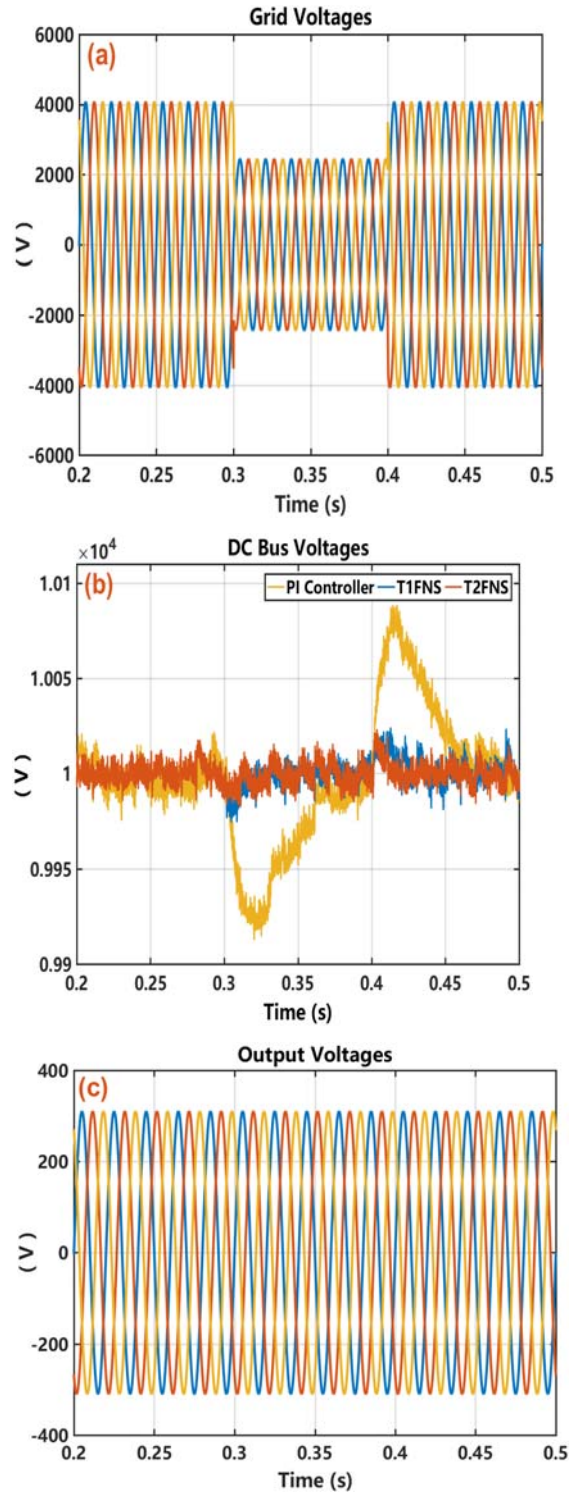


Figure 6. Waveforms obtained from the second performance test a) Grid voltages b) DC-bus voltages of input stage c) Output voltages

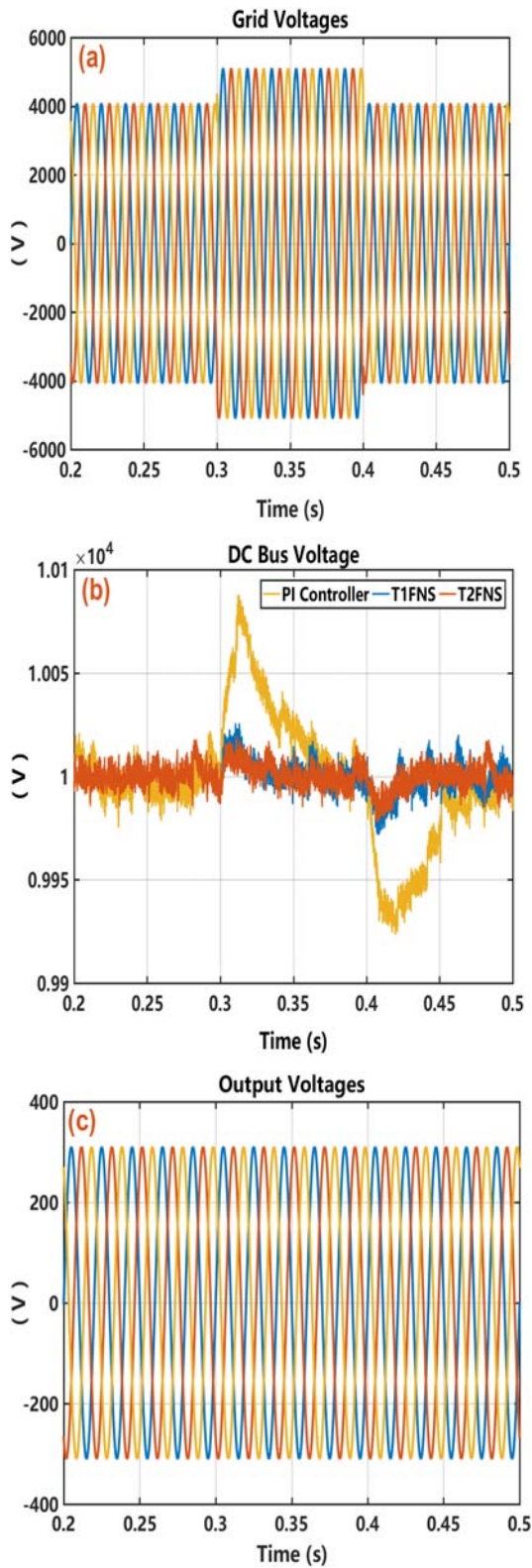


Figure 7. Waveforms obtained from the third performance test a) Grid voltages b) DC-bus voltages of input stage c) Output voltages

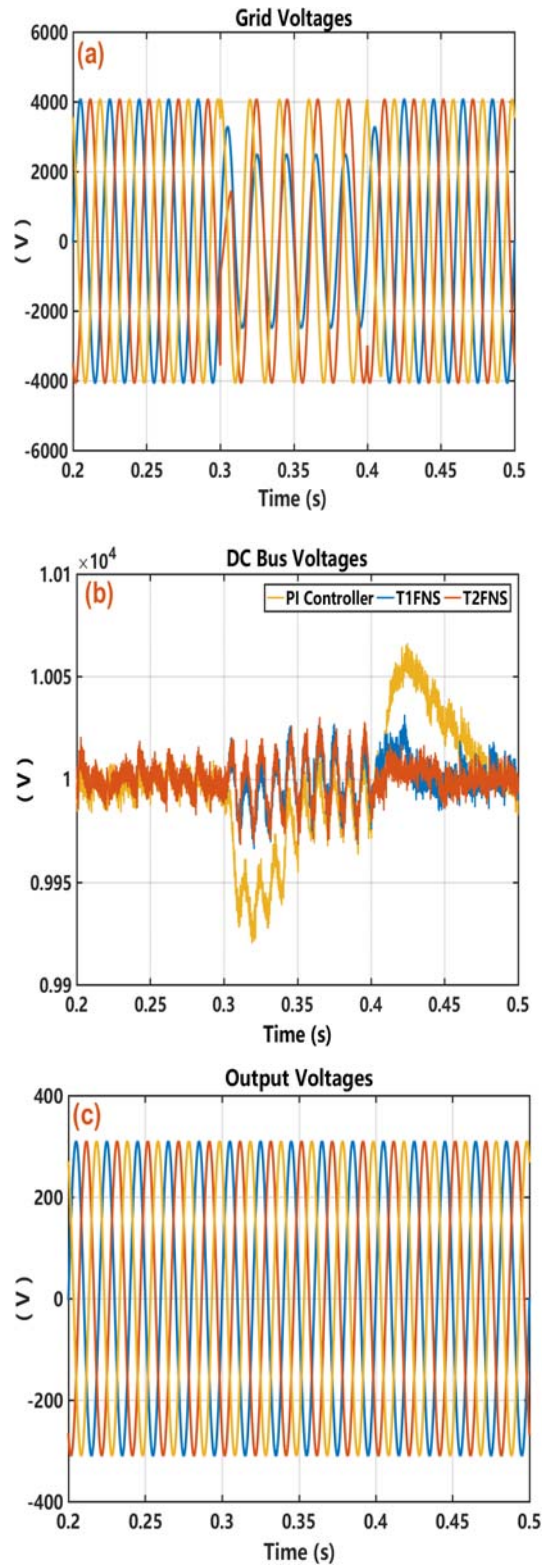


Figure 8. Waveforms obtained from the last performance test a) Grid voltages b) DC-bus voltages of input stage c) Output voltages

REFERENCES

1. Acikgoz, H., Kececioglu, O. F., Yildiz, C., Gani, A. & Sekkeli, M. (2016). Performance analysis of electronic power transformer based on neuro-fuzzy controller, *SpringerPlus*, 5(1), pp. 1-21.
2. Begian, M. B., Melek, W. W. & Mendel J. M. (2008). Parametric design of stable type-2 TSK fuzzy systems, Annual Meeting of the North American Fuzzy Information Processing Society (pp. 1–6).
3. Benzerafa, F., Tlemçani, A. & Sebaa, K. (2016). Type-1 and Type-2 Fuzzy Logic Controller Based Multilevel DSTATCOM Using SVM, *Studies in Informatics and Control*, vol. 25(1), pp. 87-98.
4. Falcones, S., Mao, X. & Ayyanar, R. (2010). Topology comparison for solid state transformer implementation, *Power and Energy Society General Meeting* (pp. 1-8).
5. Hooshmand, R. A., Ataei, M. & Rezaei, M. H. (2012). Improving the dynamic performance of distribution electronic power transformers using sliding mode control, *Journal of Power Electronics*, 12(1), pp. 145-156.
6. Jonas, E. H. & Johann, W. K. (2014). Volume/weight/cost comparison of a 1MVA 10 kV/400 V solid-state against a conventional low-frequency distribution transformer, *Energy Conversion Congress and Exposition* (pp. 1-8).
7. Karnik, N. N., Mendel, J. M. & Liang, Q. (1999). Type-2 Fuzzy Logic Systems, *IEEE Transactions on Fuzzy Systems*, 7(6), pp. 643-658.
8. Liang, Q. & Mendel, J. M. (2000). Equalization of nonlinear time-varying channels using type-2 fuzzy adaptive filters, *IEEE Trans. Fuzzy Syst.*, 8(5), pp. 551-563.
9. Liu, B., Zha, Y. & Zhang, T. (2017). D-Q frame predictive current control methods for inverter stage of solid state transformer, *IET Power Electronics*, 10(6), pp. 687-696
10. Liu, H., Mao, C., Lu, J. & Wang, D. (2009). Optimal regulator-based control of electronic power transformer for distribution systems, *Electric Power Systems Research*, 79(6), pp. 863–870.
11. McMurray, W. (1970). Power converter circuits having a high-frequency link, *U.S Patent*. 3.517.300.
12. Mendel, J. M. & John, R.I.B. (2002). Type-2 Fuzzy Sets Made Simple, *IEEE Transactions on Fuzzy Systems*, 10(2), pp. 117-127.
13. Rahib Hidayat, A. & Kaynak, O. (2010). Type 2 fuzzy neural structure for identification and control of time-varying plants, *IEEE Transactions on Industrial Electronics*, 57(12), pp. 4147-4159.
14. Tuncer, S. & Dandil, B. (2008) Adaptive neuro-fuzzy current control for multilevel inverter fed induction motor, *COMPEL*, 27(3), pp.668–681.
15. Zadeh, L. A. (1965). Fuzzy sets, *Information and Control*, 8(3), pp. 338-353.